
Article:
Emerson, N.J., Offiah, A.C. orcid.org/0000-0001-8991-5036, Reilly, G.C. orcid.org/0000-0003-1456-1071 et al. (1 more author) (2013) Patient-Specific Finite Element Modelling and Validation of Porcine Femora in Torsion. Strain, 49 (3). pp. 212-220. ISSN 0039-2103

https://doi.org/10.1111/str.12029

---

strain
An International Journal for Experimental Mechanics

Patient-Specific Finite Element Modelling and Validation of Porcine Femora in Torsion

Journal:	*Strain*
Manuscript ID:	Draft
Manuscript Type:	Full Paper
Date Submitted by the Author:	n/a
Complete List of Authors:	Emerson, Nick; The University of Sheffield, Mechanical Engineering Offiah, Amaka; Sheffield Children's NHS Foundation Trust, Academic Unit of Child Health Reilly, Gwendolen; The University of Sheffield, Engineering Materials Carre, Matt; The University of Sheffield, Mechanical Engineering
Keywords:	Finite Element, Torsion, Porcine, Bone, Femur, Simulation, Non-accidental Injury

Category:

Original Article

Title:

Patient-Specific Finite Element Modelling and Validation of Porcine Femora in Torsion

Corresponding author:

Nicholas J. Emerson;
Dept. of Mechanical Engineering, University of Sheffield, Mappin Street, Sheffield, S1 3JD, UK

Co-authors:

Amaka C. Offiah;
Academic Unit of Child Health, Sheffield Children's NHS Foundation Trust, Western Bank, Sheffield, S10 2TH, UK

Gwendolen C. Reilly;
Dept. of Engineering Materials, Kroto Research Institute, University of Sheffield, Broad Lane, Sheffield, S3 7HQ, UK

Matt J. Carré;
Dept. of Mechanical Engineering, University of Sheffield, Mappin Street, Sheffield, S1 3JD, UK

Keywords;

Finite Element; Mechanical Model; Torsion; Bone; Porcine; Femur

Word Count;

Total: 6,134

General Statement:

All authors listed within this work were fully involved in the study and preparation of the manuscript and the material within has not been and will not be submitted for publication elsewhere.

Patient-Specific Finite Element Modelling and Validation of Porcine Femora in Torsion

Nicholas J. Emerson[3], Amaka C. Offiah[1], Gwendolen C. Reilly[2], Matt J. Carré[3]*

[1]Academic Unit of Child Health, Sheffield Children's NHS Foundation Trust, Western Bank, Sheffield, S10 2TH, UK
[2]Dept. of Engineering Materials, Kroto Research Institute, University of Sheffield, Broad Lane, Sheffield, S3 7HQ, UK
[3]Dept. of Mechanical Engineering, University of Sheffield, Mappin Street, Sheffield, S1 3JD, UK

Abstract

The continued development of Finite Element (FE) modelling techniques has allowed the creation of three-dimensional models from medical data including high resolution Computed Tomography (CT). This technique has been used to assess numerous parameters, including the mechanical properties of bone, fixation techniques post-fracture and the performance of bone microarchitecture.

In this study, a semi-automated process for converting CT data into FE models has been used to model the mid-shaft (diaphysis) of porcine femoral samples under torsional load. To investigate if the all-important geometry and material property mapping functioned correctly, extensive physical validation was undertaken.

Porcine femoral specimens were imaged using contiguous helical CT, allowing the creation of an FE model using Simpleware Inc.'s ScanIP software. Inhomogeneous material properties were estimated using density-elasticity relationships proposed in literature for human samples.

Laboratory testing performed favourably, with a linear strain response validating the use of the array of linear material models used in simulation. The simulation procedure also performed well. Linear regression and mean error calculation demonstrated accurate correlation between predicted and observed results that offered improvement over the accuracy detailed within comparative testing for human samples.

Using finite element modelling on a patient-specific basis offers potential in a number of scenarios, including the determination of injury risk and design of protective equipment and mitigation of injury. The reduced ethical impact of animal samples allows for large scale fracture testing of complex loading mechanisms and the potential to consider younger animal samples (to investigate the behaviour of developing bone). Spiral fractures of long bones have been demonstrated to be an indicator of non-accidental injury in children. Combining the increased accuracy in torsional simulation in this study with younger sample testing may be employed to attempt to determine the causes of fracture from post fracture scans, aiding in the diagnosis of non-accidental injury.

Keywords; Finite Element; Mechanical Model; Torsion; Bone; Porcine; Femur

* Corresponding author. Tel.: 0114 227877; fax: 0114 227890; *E-mail address*: n.emerson@sheffield.ac.uk;

1 Introduction

Biomechanical Finite Element (FE) modelling has been under continuous development through the improvement of modelling technology and simulation techniques. The ultimate aim for biomechanical simulation of bone is the assessment of failure load and fracture risk. Determining patient-specific fracture risk has a variety of potential uses, and could be applied to increase the understanding of the causes of bone injury or to reduce the specific fracture risk of a given loading scenario or patient condition.

Geometrical accuracy in bone simulation has been improved significantly through the use of medical data as an image source. Using modern Computed Tomography (CT) as a reference medium allows the modeller to not only increase the rate at which FE models are constructed, but also to increase the accuracy of the 3D representation and to model on a patient-specific basis [1, 2]. An additional but important benefit attributed to using CT data is that the apparent density of the scanned item can be linked to the attenuation (voxel brightness) displayed within the image. With an appropriate density-elasticity relationship, the attenuation data contained within the original images can then be used to 'map' an appropriate value for Young's Modulus to each voxel within the scanned bone. Using this technique allows fine control of the applied material properties, providing an accurate estimation of the inhomogeneous material properties of a given sample.

Whilst the development and validation of bone modelling techniques has been extensive, studies have focussed primarily on human femoral samples notably the proximal region. In addition studies have considered applied loading from a single load cell in a single axis. A recent review of the development of human bone modelling recommended the extension of validation to long bones other than femurs and alternative fracture modes, including the investigation of fracture through torsion [3].

The aim of this study was to utilise the generalised techniques and procedures derived in literature to determine if the CT based FE methodology (CT-FE) is applicable when testing non-human samples in torsion. Torsion was initially selected as this represents a relatively common long bone injury, particularly at the lower extremities. Additionally, in the upper limbs of children, torsional fracture is a potential signifier for non-accidental injury [4]. The injury (either accidental or not) regularly occurs from a 'twisting' motion, with one extremity constrained and the forced, as was assessed in this study [5-7]. Additional physical and computational testing was to be undertaken in compression to compare the accuracy of the observed results for porcine samples with similar testing for human bone.

If demonstrated to be accurate, this study provides a validated methodology to extend physical validation and testing into more ethically-sensitive bone types, such as young and developing bone. The reduced ethical considerations of animal substitution and the similarities in construction to human bone have been exploited in many studies but, to date, outside of the remit of CT-FE simulation [8, 9]. Fully developed animal samples for future testing could also be selected to negate the effects of ageing that are regularly observed within cadaveric samples from older humans [10].

2 Materials and Methods

2.1 Creation of the Finite Element Model.

Porcine femoral samples were selected for testing as they offer ease of accessibility and have comparative geometry to human bone, with similar cortical and metaphyseal construction [11]. Samples were obtained from the same breeding source, aged approximately 6 months at the time of slaughter (typical slaughter weight of 55-65kg). Each sample was numbered, wrapped with saline soaked cloth and frozen (temperature approximately -20 degrees centigrade) following best practice as detailed in literature [12]. Prior to CT scanning, the samples were slowly defrosted to ambient temperature (18 +/- 5 degrees centigrade), at which point all soft tissue was removed from the surface with a scalpel.

The samples were scanned individually with the inclusion of a Mindways Calibration Phantom using a Lightspeed Volumetric CT Scanner from GE Healthcare [13] at Sheffield Children's Hospital. Dosage and scan type were set using the predetermined 'lower extremity bone' setting, which offers contiguous helical scan acquisition (arbitrary slice thickness/voxel size of 0.3125 mm) at a relatively low dosage (100kv/50mA). The inclusion of a calibration phantom aids in the analysis of apparent density of items within the scanned image, allowing accurate calculation of material properties and a means to correct unwanted scanning discrepancies between independent scans.

Fig. 1. An example mask ready to be cropped for exportation and analysis. Cutaways in the axial plane detail the meshing arrangement at the extremities and within the mid-shaft.

The scan data was imported into Simpleware's ScanIP software and masked using greyscale-based 'thresholding'. Thresholding is similar to the 'windowing' process used by clinicians to show discrete regions of soft tissue, fat, bone etc. In this case, the three dimensional mask was attributed only to voxels falling within the predefined region of greyscale values that correspond to bone. This selected the geometry required and omitted any remaining lower density soft tissues. Following this automated process, the mask was checked both visually and physically (via comparison of the modelled dimensions to the physical dimensions of the sample) to ensure accuracy was retained. Fig 1. shows a three dimensional meshed mask of a single porcine femur, prior to the isolation and exportation of the diaphysis section for simulation.

The Automated Mesh Generation algorithms (AMGs) within the software package were subjected to significant investigation to determine the most appropriate balance of modelling resolution and solve time. The FE Free algorithm was ultimately selected; this provides tetrahedral meshing throughout the mask volume, with automated refinement and re-meshing at regions of interest. The appropriateness of various AMGs has been considered in literature [14]. Viceconti et al. described tetrahedral meshing as '*probably the best method when a solid model of the target object is available'*. The precise meshing parameters varied between the models due to the differing physical dimensions of each

sample and the point at which each is constrained. Typically, the cropped models contained 550,000 high order (an additional node is included at the mid-point of each element edge) 10-noded tetrahedral elements, providing approximately 4 million degrees of freedom. The meshing procedure provided approximately 10 elements across the depth of the wall of the diaphysis, significantly improving upon the meshing resolution of previous studies in human femoral samples [15].

2.1.1 Porcine Material Properties

Material property mapping was undertaken using a two-part process. First, a linear relationship was utilised to convert the greyscale attenuation of the each voxel in the source image to a value for apparent density [16]. A density-elasticity relationship was then employed, mapping a value for Young's Modulus to each voxel. The most appropriate density-elasticity relationship for human samples has had significant investigation [17, 18]. However, despite regular substitution for human bone in physical testing, at the time of testing there was limited published information defining the material properties of porcine bone and even less consideration for a porcine density-elasticity relationship.

A review of the relationships for human bone was undertaken to determine which were capable of defining the correct elasticity at a given density for porcine cortical bone (density and elasticity were defined as proposed in literature [19] and through physical 3-point bend testing of selected cortical samples). From this correlation, three relationships were observed as appropriate, these were then used during simulation to confirm the simulation accuracy provided by each [20-22]. Fig. 2. provides a visualisation of the general mapping technique, showing the mapped elasticity on a coloured contour basis. Due to the lack of correlation with apparent density or other material quality, a single value for Poisson's Ratio was attributed to the model as a whole, regardless of greyscale attenuation. Throughout testing this was mapped with a constant value of 0.3, the average value proposed for cortical bone in human studies [23].

Fig. 2. Cutaway sections in the coronal and axial panes demonstrate the inhomogeneous distribution of elastic moduli throughout the mask volume. (Young's Modulus – MPa).

3.1 Laboratory Testing

Mechanical testing and validation was undertaken using the 'Arbitrary Strain Path 2' (ASP) rig within the Institute for Microstructural and Mechanical Process Engineering at The University of Sheffield (IMMPETUS). The test rig uses servo-controlled hydraulic actuators to provide load through a large range of strain rates, which can be undertaken in multiple axes at the same time. Data was continually sampled during testing for axial position, axial load, rotational position and torque at a sample rate of approximately 102 Hz.

Constraints were constructed within which the metaphyses of the femoral samples could be potted. Potting allows for isolation of the diaphysis, provides the opportunity for the correct alignment of the sample in all three axes and therefore reduces out-of-plane loading characteristics. Potting also provides a methodology for the application of torque to the bone extremities. The constraints were produced in two parts; a primary section that remained aligned within the test rig throughout testing, and a secondary part within which the bone was potted. This two-part testing constraint procedure represented improved methodology when compared to previous torsional fracture studies, offering a faster and more cost effective testing process [24].

Metallic, foil backed circular strain gauge rosettes were selected for strain gauged validation (Tokyo Sokki Kenkyuojo co., Ltd. – FRA-1-11-1L). Due to the constant curvature and varying geometry of the sample surface, gauges with the smallest available gauge length (1 mm) were selected. The gauges were bonded at regions of interest, as determined by cursory modeling and initial fracture testing within the laboratory.

Fig. 3. The location of the three strain gauge rosettes on the anterior and posterior surfaces. The grey sections at the extremities represent the regions potted within the constraints.

The gauges were bonded to the proximal anterior surface, the proximal medial surface in line with the midpoint of the femoral head and towards the distal end of each sample between the posterial and lateral surfaces. Three strain gauge rosettes were utilised for each bone sample, totaling nine individual gauges for each sample test. The sample preparation and gauge application methodology followed that proposed in literature [25]. The region identified for gauging was checked to ensure that the scalpel scraping had not scratched or deformed the local surface and then sanded to minimize local surface roughness. The surface was then cleaned with an alcoholic cleansing wipe to remove any surface grease. A single component cyanoacrylate bonding agent was used, offering a cold cure and therefore minimising unwanted thermal effects. A small amount of the agent was employed to fill the local pores and seal the surface of the bone to prepare for the gauge application. A further amount was then added directly to the gauge surface, and the gauge applied to the sample. The bonding agent was allowed sufficient time for curing before physical testing.

4 Testing Procedure

4.1 Physical Loading

Prior to strain gauged testing, a number of un-gauged samples were tested to fracture to determine the average fracture point in both torsion and compression. The maximum loading interval in sub-maximal testing was therefore selected as 40 Nm (significantly below the average fracture load of 78.8 Nm) for torsional testing, and 2 kN for compressive testing (fracture load average 10.3 kN).

The primary constraints were then attached to the ASP rig and appropriately aligned. The pre-gauged samples (within the secondary constraints) were placed within the primary constraint.

Initial load was applied to 50% of the maximum load interval and then released, such that the samples were centered within the two-part constraint. An accurate 'zero-point' was then determined and the gauges reset with no applied torque or compressive force. The samples were unconstrained in the z-axis throughout torsional testing to allow for vertical expansion. Correspondingly, rotation of the proximal extremity was permitted during compressive testing. The samples were allowed to 'recover' at the zero load point for approximately three minutes before loading to the next interval. The strain gauges were reset prior to each testing interval.

Following loading, all force was removed for a period of approximately three minutes, during which the strain readings were reviewed to ensure that the sample had returned to its original position and zero load state. Samples were loaded in independent intervals at 5, 10, 20, 30 and 40 Nm in torsion and to intervals of 0.5, 1, 1.5 and 2 kN in compression.

Load was implemented using strain rate control at a rate of 0.1 deg/s for all torsionally tested samples and at 0.1 mm/s for compressive tests. This pseudo-static torsional testing procedure is not strictly pure torsion, but rather defined as a 'twist' test, with one end of the sample rotated whilst the other remains fixed [26]. This loading regime is more representative of fracture *in vivo*, where one extremity is commonly observed to be constrained, whilst the other extremity is rotated or compressed.

4.2 Computational Loading

Physical testing included isolation of the diaphysis via potting of the metaphyseal regions. This ensured that the test procedure examined loading and fracture of the mid-shaft cortical bone only, fully constraining the extremities. In order to match the tested geometry, the data exported into the FE solver was cropped at the point of entry to the potting medium. Spatial registration was undertaken through the re-scanning of each sample using the initial CT scanning protocol.

Despite the significant visual effects of metallic artefacts (the constraints cause streaking of the CT image by blocking the X-ray beam), the orientation of the bone and the position relative to the test constraints were clearly notable in post-test scans.

The post-test scans were converted into three-dimensional masks, using the original thresholding protocol used to define the preliminary bone mask. The clean pre-test scan was overlaid over the post-test scan, noting the rotation and translation required to obtain the correct positioning. The point at which the sample entered the potting medium was noted, at which the point the Finite Element model was cropped. The distance from the larger artefact locations allowed the position of the gauges on the sample surface to be accurately defined. These were indicated within the simulated model through the inclusion of markers at the sample surface, which were used as indicators only, and omitted from simulation.

The cropped geometry was then imported into the FE solver (Ansys Inc.). One end of the sample was completely constrained and force was applied to the other through the inclusion of opposing couples or direct application of force upon nodes at the proximal surface. The strain gauges were intentionally positioned away from the constrained and forced regions, thus the local effects of loading the FE model in this manner were mitigated. The material markers outputted from the density-elasticity relationships are linear in nature, which provided a correspondingly linear response to increased loading.

Localised results between computation and physical testing were compared using the methodology detailed by Taddei et al. [25]. The local material property for each gauge location was extracted from the finite element model and was used to determine the principle stresses from the rosette results. This ensured that the inhomogeneous nature of the bone material was accounted for in test result comparisons, ensuring accuracy within the high stress gradients noted between neighbouring regions.

Parameter identification and rationalisation was undertaken via iterative modelling of the samples, such that the importance and effect of changing input parameters could be assessed. Tested parameters included the selected material relationship, meshing protocols and the alignment and the manner in which force was applied to the model. In total, three material relationships that had been derived for human samples were considered, and the accuracy of each was determined though simulation [21, 27, 28]. Fig 4. shows the changing level of correlation observed for the same laboratory results from a single femur under torsion when simulated using the three material relationships.

Fig. 4. A comparison of the predicted vs. observed agreement for the three material relationships for a single sample under torsion.

5 Results

5.1 Physical Testing

The strain gauge results demonstrated clear linearity (as denoted by R^2 value > 0.99) in all locations for the majority of loading intervals. Slight departure from linearity (as noted by $R^2 < 0.95$) was observed in a small number of cases (4 out of a total of 36 gauges) reporting strain readings of less than 50 microstrain. Strain readings demonstrated a swinging variation of approximately +/- 8 microstrain. Consequently, the departure from linearity is likely to be due to the lower absolute results, of which the inaccuracy in reading represents a bigger proportion. There was no correlation observed in the polarity or value of these discrepancies; it should be noted that the errors represented a low proportion of the absolute strain reading (typically less than 8% variation).

Neither repeated testing nor changing of the loading regime demonstrated evidence of plastic deformation, and reloading to the same interval twice demonstrated only slight variation between re-reads in all locations. Examination of the load-deflection curve in showed no permanent creep within

sub-maximal testing. The linearity and repeatability of the test results validated the use of linear material models for whole-bone porcine simulation.

Brittle, elastic failure was noted for all samples that were tested to fracture. In torsion, the fracture type was immediately visible as a spiral fracture, spanning the length of the exposed diaphysis. Maximum permissible torque within the fractured samples ranged from 59.7 to 94.1 Nm (Av. 78.8 Nm), maximum deflection of the samples ranged from 11.5 to 15.8 degrees (Av. 13.1 degrees). Linearity was observed in the load/deflection plots of all fractured samples (typical R^2 value > 0.99) until 85-90% of maximal loading. An increase in strain rate was then typically observed at the onset of yield, until total fracture was determined, as indicated by a sharp increase in strain rate, a reduction of load at the crosshead, and an audible break. Failure in compression was also noted as elastic and brittle, with failure load ranging from 9.3 to 11.9 KN (Av. 10.3). Maximum vertical deflection ranged from 5.68 to 7.89 mm at total failure (Av. 7.0 mm)

5.2 Predicted Versus Observed Results

Results were obtained on a pseudo-static basis for both the laboratory testing and simulation. The linearity of the strain results was retained and repeatable for discrete tests and the load deflection curves showed no significant plastic deformation during testing. Consequently, the individual results were considered as independent entities and values from differing samples could be compared simultaneously to consider the accuracy of the simulation process as a whole.

The strain gauging results were observed in the form of a comparison of maximum and minimum principal stress. This approach was undertaken to accommodate for the manner in which the modelling procedure plots material properties. Principal stress results were obtained for the finite element model at all nodes directly beneath the sensing area of the strain gauge rosette to a depth of approximately 2mm, and then averaged. This mimics the manner in which the strain gauge averages the strain result over the length of the gauge and accounts for the changing material properties observed away from the surface. Comparing the maximum and minimum principal stresses at each gauge location and each loading interval provided a total of 108 individual data points that were used for validation of the FE process.

The results for maximum and minimum principal stress illustrated in fig 4. & fig. 5. are in the format of *predicted vs. observed* stress. The ideal result from this would be that the results describe a line of equation $x = y$ with the intercept at 0,0 and minimal deviation of the data points from this ideal line, as denoted by an R^2 value approaching unity. To observe the behaviour of the samples at each specific gauge location and in discrete loading intervals, the error of each data point was assessed in terms of peak error, and averaged error (Root Mean Square Error - RMSE).

The parameter identification process demonstrated that the relationship proposed by Morgan et al. provided the most accurate agreement. This is a result that has been previously demonstrated in

literature for human but importantly was confirmed as the most appropriate general relationship for porcine samples [29].

The combined results are detailed in fig. 5. allowing direct comparison of the testing technique as a whole. The details of the linear regression calculation are displayed within the plot, as are the results of the error calculations. As can be seen, the data points of the graph plot to a line that is close to the ideal gradient of unity with a high level of fit ($R^2 = 0.950$).

Peak error in terms of absolute values for a single observed compared to a single predicted result was 12.2 MPa (-40.22 MPa Observed, -52.39 MPa Predicted). In percentage terms the peak error was a 127.1% under prediction (2.5 MPa Observed, 5.7 MPa Predicted). Root Mean Squared Error in absolute terms was noted as 3.4 MPa, which represents 7.4 % of the maximum observed value.

The maximum percentage error was observed for a measured result of –2.5 MPa, which is the third lowest result observed throughout the entire testing procedure and thus potentially more susceptible to increased error, particularly on a percentage basis.

Fig. 5. A comparison of the predicted vs. observed principal stress for the entire validation process. The dashed blue line shows the ideal result.

The verification in terms of principal stress that was undertaken in this study followed the methodology originally determined by Lengsfeld et al., Dalstra et al. and Taddei et al. [30-32]. This ensured that the processes used had been previously considered and were valid for the accurate testing of bone samples. Using confirmed techniques also allowed for the direct comparison of the accuracy obtained within this study with that detailed in literature. Taddei et al. (whose study was the most recent) tested a single human femoral sample under compressive force applied at varying angles to obtain stress results for different loading conditions. The process used by Taddei et al. was considered as the most appropriate for the comparison of stress-based accuracy, as this paper was subsequently used as the basis for further investigation of additional aspects of the CTFE process in human sample modelling, such as material mapping strategy and the selected density – elasticity relationship [18, 33]. Table 1 shows a comparison of the overall accuracy, agreement and error between the results observed for porcine testing, and the results obtained by Taddei et al.

Of particular note in the table is the starred item (*) for maximum error. Taddei et al. reported a maximum error of 27%, which, whilst not explicitly stated, seems to relate to the maximum absolute error, correlated to the maximum absolute stress result observed in the study as a whole. On which basis, the maximum error in this study would not represent the 127.1% error reported (5.7 MPa predicted to 2.5 MPa observed) but be significantly reduced to 26.3% (12.2 MPa maximum error to 46.2 MPa maximum observed result).

Table. 1. A comparison of the agreement and error between the results observed for porcine testing in this study, and the results obtained using similar techniques human femur testing.

6 Discussion

The aim of this study was to investigate the substitution of animal samples in CT-FE simulation, and furthermore to consider the simulation of torsional loading. Following the destructive testing of fifteen porcine femoral samples, two further samples were selected for strain gauged investigation. This provided 108 individual data points from nine different loading intervals which were used to compare the predicted principal stress with those measured in the laboratory.

The main findings of the study are that animal substitution (specifically porcine substitution) can be undertaken with comparative accuracy to that published for human samples. In addition, density-elasticity relationships derived for human samples are demonstrated to be appropriate for porcine simulation. As with the simulation of human samples, the mapping relationship used was shown to have an effect on the observed results, with the relationship proposed by Morgan et al. proving most suitable.

Laboratory testing performed favourably, demonstrating linearity of the strain gauge results, and a lack of plastic deformation in repeated loading sub maximal loading. This result is critical when modelling a structure using linear elastic models. Further support was provided through investigation of the load /deflection plots for the samples taken to complete fracture, which showed no departure from linearity in general, although a distinct yield point was generally discernible at some non-linearity was noted approaching the fracture point (typically around 86% of the total fracture load) .

The variation in fracture load observed in physical testing can be attributed to the varying geometry between samples. Despite the samples being from a single source, reared concurrently and slaughtered at the same age, there was notable geometrical variation between test pieces in all dimensions. This further demonstrates the need for patient-specific modelling, allowing even small variations in geometry and apparent density to be accommodated on a patient by patient basis. Whilst there was no influence upon the production or rearing of the animals as part of this study, the animals were confirmed to have been reared using the same diet. This, in theory, reduces any effect of diet on material properties as observed by Crenshaw et al. [34]. The manner in which the subjects failed, and the prediction of the point of failure of additional samples is a subject of further investigation. The elastic, brittle fracture noted throughout this study signified failure through the reaching of an ultimate strain limit, as proposed by Bayraktar et al. [35].

Despite high levels of correlation accuracy in validation, evidence of a slight dichotomy is noted in the negative aspect of the results. This was shown to be for a single femur, rather than describing the difference between the two gauged femora, suggesting that misalignment of the sample or the locating

of a strain gauge rosette may be responsible. Parameter identification demonstrated the importance of the alignment of the model and the finite element model boundary conditions. Accuracy may be improved and error reduced with a revision of the spatial registration methodology. For example, moving from post-testing spatial registration to a live system during testing could potentially increase the simulation accuracy.

In summary, successful validation and preliminary fracture testing shown in this study has demonstrated that the substitution of animal bone is not only applicable, but also capable of yielding accurate results. The level of geometrical accuracy and meshing refinement utilised are likely to be contributors to the high levels of accuracy achieved.

Expansion of the testing protocol to consider alternative testing methodologies, including alternative loading regimes, developing bone samples and improved spatial registration should be examined in due course. Additionally future studies will attempt to increase the predictive aspect of simulation, estimating the torsional load required to fracture a sample from the original CT data. Should the level of accuracy observed in this validation study be maintained in fracture prediction, the process has significant potential in both industry and product design, and on a clinical basis. In particular, combing the understanding of fractures caused by a 'gripping' or 'twisting' motion with the analysis of developing bone has the potential to aid in the understanding of non-accidental injury in children.

Acknowledgements

The authors gratefully acknowledge the funding of the EPSRC, and Simpleware Ltd. for their assistance in this project. Thanks are extended to Ms Yvonne Vickers, Superintendent Radiographer, Sheffield Children's Hospital and John Middlemiss and Brad Wynne of the IMMPETUS Team at The University of Sheffield for their the continued support and assistance.

Conflict of Interest Statement

There are neither any financial, nor personal relationships with other investigators or organisations that could inappropriately influence this work.

References

1. *Bessho, M., et al., Prediction of strength and strain of the proximal femur by a CT-based finite element method. Journal of Biomechanics, 2007.* ***40****(8): p. 1745-1753.*
2. *Camacho, D.L.A., et al., An improved method for finite element mesh generation of geometrically complex structures with application to the skullbase. Journal of Biomechanics, 1997.* ***30****(10): p. 1067-1070.*
3. *Viceconti, M., et al., Multiscale modelling of the skeleton for the prediction of the risk of fracture. Clinical Biomechanics, 2008.* ***23****(7): p. 845-852.*

4. *Worlock, P., M. Stower, and P. Barbor, Patterns of fractures in accidental and non-accidental injury in children: a comparative study. BMJ, 1986.* ***293****(6539): p. 100-102.*

5. *Cowan, D.N., et al., Lower limb morphology and risk of overuse injury among male infantry trainees. Medicine and Science in Sports and Exercise, 1996.* ***28****(8): p. 945-952.*

6. *Novacheck, T.F., The biomechanics of running. Gait & Posture, 1998.* ***7****(1): p. 77-95.*

7. *Galano, G.J., et al., The Most Frequent Traumatic Orthopaedic Injuries From a National Pediatric Inpatient Population. Journal of Pediatric Orthopaedics, 2005.* ***25****(1): p. 39-44.*

8. *Seil, R., et al., Comparison of Initial Fixation Strength Between Biodegradable and Metallic Interference Screws and a Press-Fit Fixation Technique in a Porcine Model. The American Journal of Sports Medicine, 1998.* ***26****(6): p. 815-819.*

9. *Southern EP, O.T., Panjabi MM, Duranceau JS., Cervical spine injury patterns in three modes of high-speed trauma: a biomechanical porcine model. J Spinal Disord., 1990.* ***3****: p. 316-28.*

10. *Baumer, T.G., et al., Age Dependent Mechanical Properties of the Infant Porcine Parietal Bone and a Correlation to the Human. Journal of Biomechanical Engineering, 2009.* ***131****(11): p. 111006.*

11. *AI Pearce, R.R., S Milz, E Schneider, SG Pearce, Animal models for implant biomaterial research in bone: A review. European Cells and Materials (ECM), 2007.* ***13****: p. 1-10.*

12. *Evans, F.G., Factors affecting the mechanical properties of bone. Bull N Y Acad Med, 1973.* ***49****(9): p. 751-64.*

13. *Healthcare, G., A division of General Electric Company. 2012.*

14. *Viceconti, M., et al., A comparative study on different methods of automatic mesh generation of human femurs. Medical Engineering & Physics, 1998.* ***20****(1): p. 1-10.*

15. *Yosibash, Z., D. Tal, and N. Trabelsi, Predicting the yield of the proximal femur using high-order finite-element analysis with inhomogeneous orthotropic material properties. Philosophical Transactions of the Royal Society A: Mathematical,*

16. *McBroom, R.J., et al., Prediction of vertebral body compressive fracture using quantitative computed tomography. Journal of Bone and Joint Surgery Incorporated, 1985.* ***67****(8).*

17. *Helgason, B., et al., Mathematical relationships between bone density and mechanical properties: A literature review. Clinical biomechanics (Bristol, Avon), 2008.* ***23****(2): p. 135-146.*

18. *Taddei, F., A. Pancanti, and M. Viceconti, An improved method for the automatic mapping of computed tomography numbers onto finite element models. Medical Engineering & Physics, 2004.* ***26****(1): p. 61-69.*

19. *Bonney, H., B.J. Colston, and A.M. Goodman, Regional variation in the mechanical properties of cortical bone from the porcine femur. Medical Engineering & Physics, 2011.* ***33****(4): p. 513-520.*

20. *Lotz, J.C., T.N. Gerhart, and W.C. Hayes, Mechanical Properties of Trabecular Bone from the Proximal Femur: A Quantitative CT Study. Journal of Computer Assisted Tomography, 1990.* ***14****(1): p. 107-114.*

21. *Morgan, E.F., H.H. Bayraktar, and T.M. Keaveny, Trabecular bone modulus–density relationships depend on anatomic site. Journal of Biomechanics, 2003.* ***36****(7): p. 897-904.*

22. *Snyder, S.M. and E. Schneider, Estimation of mechanical properties of cortical bone by computed tomography. Journal of Orthopaedic Research, 1991.* ***9****(3): p. 422-431.*

23. *Wirtz, D.C., et al., Critical evaluation of known bone material properties to realize anisotropic FE-simulation of the proximal femur. Journal of Biomechanics, 2000.* ***33****(10): p. 1325-1330.*

24. *Ho, K., et al., The effect of 4 mm bicortical drill hole defect on bone strength in a pig femur model. Archives of Orthopaedic and Trauma Surgery, 2010.* ***130****(6): p. 797-802.*

25. *Taddei, F., et al., The material mapping strategy influences the accuracy of CT-based finite element models of bones: An evaluation against experimental measurements. Medical Engineering & Physics, 2007.* ***29****(9): p. 973-979.*

26. *Saunders, M.M., et al., Development of a cost-effective torsional unit for rodent long bone assessment. Medical Engineering & Physics, 2010.* ***32****(7): p. 802-807.*

27. *Keller, T.S., Z. Mao, and D.M. Spengler, Young's modulus, bending strength, and tissue physical properties of human compact bone. Journal of orthopaedic research : official publication of the Orthopaedic Research Society, 1990.* ***8****(4): p. 592-603.*

28. *Carter, D. and W. Hayes, Bone compressive strength: the influence of density and strain rate. Science, 1976.* ***194****(4270): p. 1174-1176.*

29. *Schileo, E., et al., Subject-specific finite element models can accurately predict strain levels in long bones. Journal of Biomechanics, 2007.* ***40****(13): p. 2982-2989.*

30. *Lengsfeld, M., et al., Comparison of geometry-based and CT voxel-based finite element modelling and experimental validation. Medical Engineering & Physics, 1998.* ***20****(7): p. 515-522.*

31. *Taddei, F., et al., Subject-specific finite element models of long bones: An in vitro evaluation of the overall accuracy. Journal of Biomechanics, 2006.* ***39****(13): p. 2457-2467.*

32. *Dalstra, M., R. Huiskes, and L.v. Erning, Development and Validation of a Three-Dimensional Finite Element Model of the Pelvic Bone. Journal of Biomechanical Engineering, 1995.* ***117****(3): p. 272-278.*

33. *Schileo, E., et al., Subject-specific finite element models implementing a maximum principal strain criterion are able to estimate failure risk and fracture location on human femurs tested in vitro. Journal of Biomechanics, 2008.* ***41****(2): p. 356-367.*

34. *Crenshaw, T.D., et al., Influence of Age, Sex and Calcium and Phosphorus Levels on the Mechanical Properties of Various Bones in Swine. J. Anim Sci., 1981.* ***52****(6): p. 1319-1329.*

35. *Bayraktar, H.H., et al., Comparison of the elastic and yield properties of human femoral trabecular and cortical bone tissue. Journal of Biomechanics, 2004.* ***37****(1): p. 27-35.*

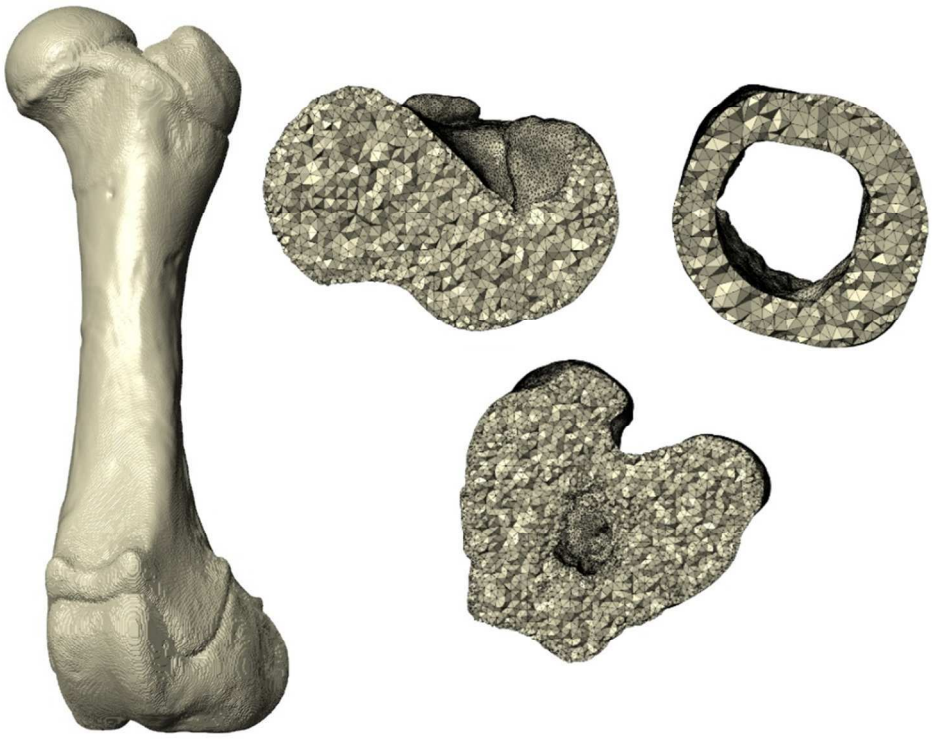

Fig. 1. An example mask ready to be cropped for exportation and analysis. Cutaways in the axial plane detail the meshing arrangement at the extremities and within the mid-shaft.
266x198mm (96 x 96 DPI)

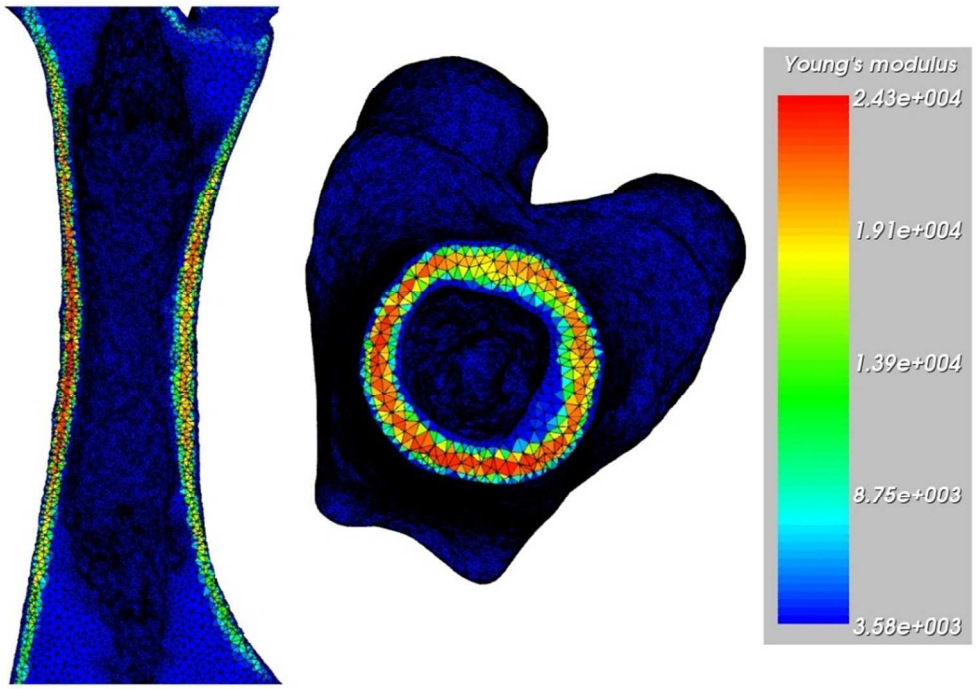

Fig. 2. Cutaway sections in the coronal and axial panes demonstrate the inhomogeneous distribution of elastic moduli throughout the mask volume. (Young's Modulus – MPa).
121x86mm (220 x 220 DPI)

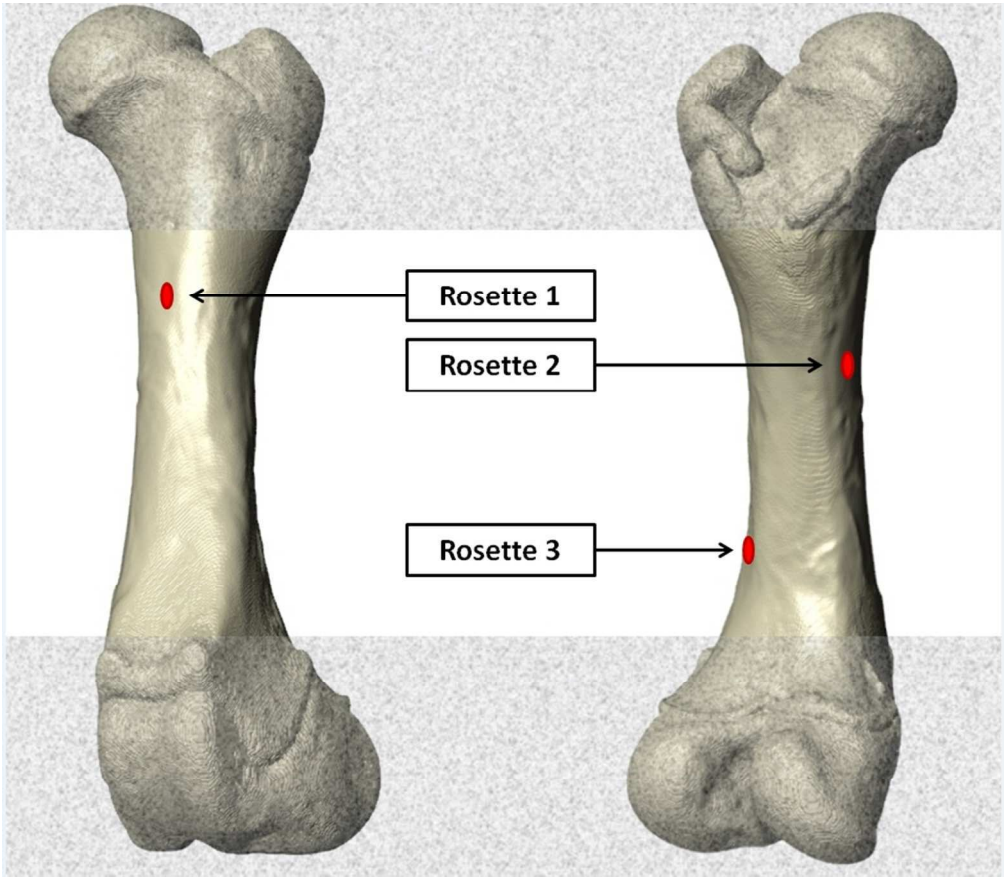

Fig. 3. The location of the three strain gauge rosettes on the anterior and posterior surfaces. The grey sections at the extremities represent the regions potted within the constraints.
252x220mm (96 x 96 DPI)

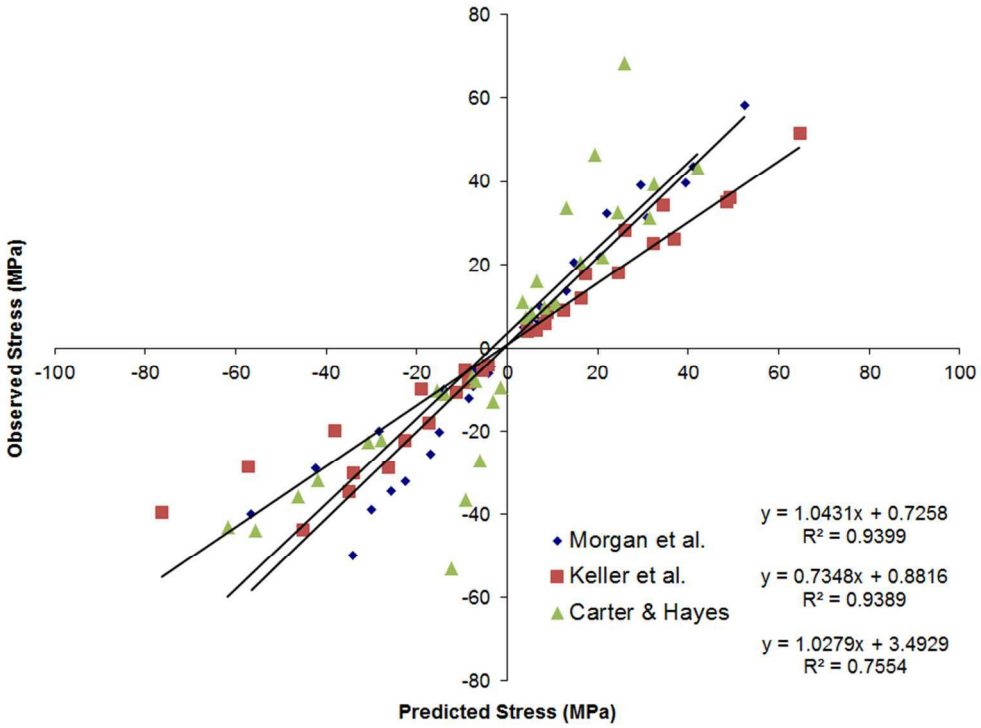

Fig. 4. A comparison of the predicted vs. observed agreement for the three material relationships for a single sample under torsion.
242x183mm (96 x 96 DPI)

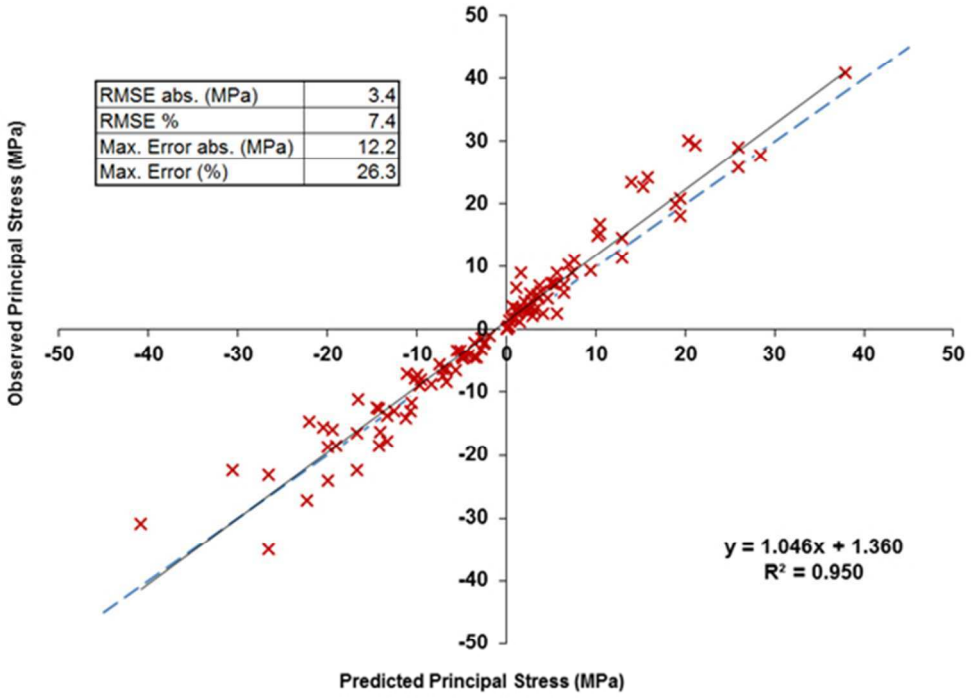

Fig. 5. A comparison of the predicted vs. observed principal stress for the entire validation process. The dashed blue line shows the ideal result.
162x124mm (96 x 96 DPI)

	Accuracy Reported by Taddei et al. [25]	Accuracy Observed in this Study
Agreement (R^2 Value)	0.91	0.95
RMSE (MPa)	2.6	3.4
RMSE (%)	8.6%	7.4%
Max. error (MPa)	8.3	12.2
Max. error (% of observed result)	27%*	127.1% / 26.3% *

Table. 1. A comparison of the agreement and error between the results observed for porcine testing in this study, and the results obtained using similar techniques human femur testing.
252x90mm (96 x 96 DPI)